

General Green's function formalism for transport calculations with *spd*-Hamiltonians and giant magnetoresistance in Co and Ni based magnetic multilayers

S. Sanvito*, C.J. Lambert†,

School of Physics and Chemistry, Lancaster University LA1 4YB, Lancaster UK

J.H. Jefferson,

DERA, Electronic and Optical Materials Centre, Malvern, Worcs. WR14 3PS, UK

A.M. Bratkovsky‡

Hewlett-Packard Laboratories, 3500 Deer Creek Road, Palo Alto, CA 94304-1392

(October 1, 2018)

A novel, general Green's function technique for elastic spin-dependent transport calculations is presented, which (i) scales linearly with system size and (ii) allows straightforward application to general tight-binding Hamiltonians (*spd* in the present work). The method is applied to studies of conductance and giant magnetoresistance (GMR) of magnetic multilayers in CPP (current perpendicular to planes) geometry in the limit of large coherence length. The magnetic materials considered are Co and Ni, with various non-magnetic materials from the *3d*, *4d*, and *5d* transition metal series. Realistic tight-binding models for them have been constructed with the use of density functional calculations. We have identified three qualitatively different cases which depend on whether or not the bands (densities of states) of a non-magnetic metal (i) form an almost perfect match with one of spin sub-bands of the magnetic metal (as in Cu/Co spin valves); (ii) have almost pure *sp* character at the

*e-mail: sanvito@dera.gov.uk

†e-mail: c.lambert@lancaster.ac.uk

‡e-mail: alexb@hpl.hp.com

Fermi level (e.g. Ag); (iii) have almost pure d character at the Fermi energy (e.g. Pd, Pt). The key parameters which give rise to a large GMR ratio turn out to be (i) a strong spin polarization of the magnetic metal, (ii) a large energy offset between the conduction band of the non-magnetic metal and one of spin sub-bands of the magnetic metal, and (iii) strong interband scattering in one of spin sub-bands of a magnetic metal. The present results show that GMR oscillates with variation of the thickness of either non-magnetic or magnetic layers, as observed experimentally.

I. INTRODUCTION

The discovery [1] of giant magnetoresistance (GMR) in metallic multilayers about a decade ago has attracted a great deal of attention. This is not only because of the possibility of building sensitive magnetometers, but also because GMR provides valuable insight into spin-dependent transport in inhomogeneous systems. GMR is the drastic change in electrical resistance that occurs when a strong magnetic field is applied to a superlattice made with alternating magnetic and non-magnetic (spacer) metallic layers. Early experiments were conducted with the so-called current-in-plane (CIP) configuration, in which the current flows parallel to the plane of the layers. In this configuration the dimensions of the system are macroscopic with transport properties being reasonably described by a classical Boltzmann equation [2] and GMR is associated with the spin-dependent scattering of electrons at the interfaces.

The first experiments with the current perpendicular to the plane of the layers (CPP) [3] paved the way to a completely different regime, where quantum effects can play a dominant role. In good quality superlattices the elastic mean free path can extend over several layers and the spin diffusion length can be longer than the total superlattice thickness. In this case we can talk, according to Mott [4], about majority and minority spin carriers as two

independent spin fluids which remain coherent as they cross the superlattice layers. Then a full quantum description is required. For such structures the magnetoconductance and GMR are found to be oscillatory functions of the non-magnetic layer thickness [5] with periods extending over several atomic planes. Despite the evidence of such important quantum effects, early theoretical work was based on spin-dependent scattering at interfaces and/or magnetic impurities and completely neglected quantum interference. In 1995 Schep et al. [6,7] challenged this conventional picture and showed that large values of GMR (of order 120%) exist even in absence of impurity scattering.

The aim of the present paper is to develop a quantitative approach to quantum transport, which describes the dependence of GMR on specific material and/or layer thickness. Our calculations are based on the Landauer-Büttiker formalism [8], using a nearest neighbor tight-binding *spd* Hamiltonian. The tight-binding energy parameters have been fitted to accurate *ab-initio* density functional calculations.

We have developed a novel and completely general technique for calculating Green functions and hence a scattering *S* matrix and transport coefficients of a finite superlattice connected to pure crystalline semi-infinite leads. This allowed us to perform a systematic study of Co/A and Ni/A multilayers, where A=Cu, Ag, Pd, Au and Pt, and analyze optimal conditions for GMR.

We shall consider below a GMR ratio of a finite superlattice connected to two semi-infinite crystalline leads [9], as sketched in Fig. 1. The GMR ratio is defined by

$$\text{GMR} = (\Gamma_{\text{FM}}^{\uparrow} + \Gamma_{\text{FM}}^{\downarrow} - 2\Gamma_{\text{AF}}^{\uparrow\downarrow})/2\Gamma_{\text{AF}}^{\uparrow\downarrow}, \quad (1.1)$$

where $\Gamma_{\text{FM}}^{\sigma}$ is the conductance of a given spin channel σ in the ferromagnetic (FM) configuration and $\Gamma_{\text{AF}}^{\uparrow\downarrow}$ is the corresponding conductance (for either spin) in the anti-ferromagnetic state. We calculate the conductance by evaluating the Landauer formula [8]

$$\Gamma^{\sigma} = \frac{e^2}{h} T^{\sigma}, \quad (1.2)$$

where T^{σ} is the total transmission coefficient for the spin σ calculated at the Fermi energy. In what follows we assume a perfect match at the interface between the fcc lattices of the

different metals. This assumption is particularly good in the case of Co, Cu, and Ni which possess almost identical lattice constants. Equation (1.2) is valid even in the presence of disorder. We shall consider below crystalline systems with smooth interfaces, where k_{\parallel} is a good quantum number (we use the symbol \parallel for the in-plane coordinates and \perp for the direction of the current). The Hamiltonian can then be diagonalized in the Bloch basis k_{\parallel} to yield

$$\Gamma^{\sigma} = \sum_{k_{\parallel}} \Gamma^{\sigma}(k_{\parallel}) = \frac{e^2}{h} \sum_{k_{\parallel}} T^{\sigma}(k_{\parallel}), \quad (1.3)$$

where the sum over k_{\parallel} is extended over the two-dimensional Brillouin zone in the case of infinite cross section and over the allowed discrete k_{\parallel} 's in the case of finite cross section.

II. GREEN'S FUNCTION FORMALISM FOR SCATTERING MATRIX.

The problem of analyzing a realistic tight-binding model, with *spd* orbitals on each site represents a formidable numerical challenge [10,11]. In this section we describe a very general and efficient technique for calculating the *S*-matrix and hence the transmission coefficients of an arbitrary scattering region such as a superlattice, attached to two semi-infinite crystalline leads. The key components of the calculation are i) the retarded Green function g of the semi-infinite leads and ii) an effective Hamiltonian H_{eff} describing the scattering region and its coupling to the leads. The approach described below provides a versatile method for computing these two components, which are then combined via Dyson's equation to yield the Green function of the complete structure. A novel feature of the technique is that it avoids adding a small imaginary part to the energy and provides a semi-analytic formula for g .

A. The Green function of an arbitrary semi-infinite lead.

To compute the Green function for a semi-infinite crystalline lead of finite cross-section, we first calculate the Green function of a doubly infinite system and then derive the semi-

infinite case by applying boundary conditions at the end of the lead. To this end, consider the doubly infinite system shown in Fig.2.

If z is the direction of transport, the system comprises a periodic sequence of slices, described by an intra-slice matrix H_0 and coupled by a nearest neighbor inter-slice hopping matrix H_1 . The nature of the slices need not be specified at this stage. They can describe a single band atom in an atomic chain, an atomic plane or a more complex cell. For such a general system, the total Hamiltonian H can be written as an infinite matrix of the form

$$H = \begin{pmatrix} \dots & \dots & \dots & \dots & \dots & \dots & \dots & \dots \\ \dots & H_0 & H_1 & 0 & \dots & \dots & \dots & \dots \\ \dots & H_{-1} & H_0 & H_1 & 0 & \dots & \dots & \dots \\ \dots & 0 & H_{-1} & H_0 & H_1 & 0 & \dots & \dots \\ \dots & 0 & 0 & H_{-1} & H_0 & H_1 & 0 & \dots \\ \dots & \dots & \dots & \dots & \dots & \dots & \dots & \dots \\ \dots & \dots & \dots & \dots & \dots & \dots & \dots & \dots \end{pmatrix}, \quad (2.1)$$

where H_0 is Hermitian and $H_{-1} = H_1^\dagger$. The Schrödinger equation for this system is of the form

$$H_0\psi_z + H_1\psi_{z+1} + H_{-1}\psi_{z-1} = E\psi_z, \quad (2.2)$$

where ψ_z is a column vector corresponding to the slice at the position z with z an integer measured in units of inter-slice distance. Let the quantum numbers corresponding to the degrees of freedom within a slice be $\mu = 1, 2, \dots, M$ and the corresponding components of ψ_z be ψ_z^μ . For example in the following sections, these enumerate the atomic sites within the slice and the valence orbitals (*spd*) at a site. The Schrödinger equation may then be solved by introducing the Bloch state,

$$\psi_z = n_{k_\perp}^{1/2} e^{ik_\perp z} \phi_{k_\perp}, \quad (2.3)$$

where ϕ_{k_\perp} is a normalized M -component column vector and $n_{k_\perp}^{1/2}$ an arbitrary constant. Substituting into the equation (2.2) gives

$$\left(H_0 + H_1 e^{ik_\perp} + H_{-1} e^{-ik_\perp} - E\right) \phi_{k_\perp} = 0, \quad (2.4)$$

Our task is to compute the Green function g of such a structure, for all real energies. For a given energy E , the first task is to determine all possible values (both real and complex) of the wavevectors k_\perp by solving the secular equation

$$\det(H_0 + H_1 \chi + H_{-1}/\chi - E) = 0. \quad (2.5)$$

where $\chi = e^{ik_\perp}$.

In contrast to conventional band-theory, where the problem is to compute the M values of E for a given (real) choice of k_\perp , our aim is to compute the complex roots χ of the polynomial (2.5) for a given (real) choice of E . Consider first the case where H_1 is not singular. We note that for real k_\perp , conventional band-theory yields M energy bands $E_n(k_\perp)$, $n = 1, \dots, M$, with $E_n(k_\perp + 2\pi) = E_n(k_\perp)$. As a consequence, for a given choice of E , to each real solution $k_\perp = k$, for which the group velocity

$$v_k = \frac{1}{\hbar} \frac{\partial E(k)}{\partial k} \quad (2.6)$$

is positive, there exists a second solution $k_\perp = \bar{k}$ for which the group velocity

$$v_{\bar{k}} = \frac{1}{\hbar} \frac{\partial E(\bar{k})}{\partial k} \quad (2.7)$$

is negative. These real wavevectors define the open scattering channels of the structure and in the simplest case, where $H_1 = H_{-1}$, one finds $k = -\bar{k}$. We also note that to each solution k_\perp the Hermitian conjugate of (2.4) shows that k_\perp^* is also a solution. Hence to each “right-decaying” solution k possessing a positive imaginary part, there is a “left-decaying” solution \bar{k} with a negative imaginary part. For the purpose of constructing the Green function, this leads us to divide the roots of (2.4) into two sets: the first set of M wavevectors labeled k_l ($l = 1, \dots, M$) correspond to right-moving and right-decaying plane-waves and the second set labeled \bar{k}_l ($l = 1, \dots, M$) correspond to left-moving and left-decaying plane-waves.

Although the solutions to (2.5) can be found using a root tracking algorithm, for numerical purposes it is more convenient to map (2.4) onto an equivalent eigenvalue problem by introducing the matrix \mathcal{H}

$$\mathcal{H} = \begin{pmatrix} -H_1^{-1}(H_0 - E) & -H_1^{-1}H_{-1} \\ \mathcal{I} & 0 \end{pmatrix}, \quad (2.8)$$

where \mathcal{I} is the M dimensional identity matrix. The eigenvalues of \mathcal{H} are the $2M$ roots e^{ik_l} , $e^{i\bar{k}_l}$ and the upper M components of the eigenvectors of \mathcal{H} are the corresponding eigenvectors $\phi_{k_l}, \phi_{\bar{k}_l}$.

To construct the retarded Green function $g_{zz'}$ of the doubly infinite system, we note that except at $z = z'$, g is simply a wavefunction and hence must have the form

$$g_{zz'} = \begin{cases} \sum_{l=1}^M \phi_{k_l} e^{ik_l(z-z')} \mathbf{w}_{k_l}^\dagger & z \geq z' \\ \sum_{l=1}^M \phi_{\bar{k}_l} e^{i\bar{k}_l(z-z')} \mathbf{w}_{\bar{k}_l}^\dagger & z \leq z' \end{cases} \quad (2.9)$$

where the M -component vectors \mathbf{w}_{k_l} and $\mathbf{w}_{\bar{k}_l}$ are to be determined. Since $g_{zz'}$ is retarded both in z and z' , it satisfies the Green function equation corresponding to (2.2) and is continuous at the point $z = z'$, one obtains

$$g_{zz'} = \begin{cases} \sum_{l=1}^M \phi_{k_l} e^{ik_l(z-z')} \tilde{\phi}_{k_l}^\dagger \mathcal{V}^{-1} & z \geq z' \\ \sum_{l=1}^M \phi_{\bar{k}_l} e^{i\bar{k}_l(z-z')} \tilde{\phi}_{\bar{k}_l}^\dagger \mathcal{V}^{-1} & z \leq z' \end{cases}. \quad (2.10)$$

The matrix \mathcal{V} is defined by

$$\mathcal{V} = \sum_{l=1}^M H_{-1} \left[\phi_{k_l} e^{-ik_l} \tilde{\phi}_{k_l}^\dagger - \phi_{\bar{k}_l} e^{-i\bar{k}_l} \tilde{\phi}_{\bar{k}_l}^\dagger \right], \quad (2.11)$$

and the set of vectors $\tilde{\phi}_{k_l}^\dagger$ ($\tilde{\phi}_{\bar{k}_l}^\dagger$) are the duals of the set ϕ_{k_l} ($\phi_{\bar{k}_l}$), defined by

$$\tilde{\phi}_{k_l}^\dagger \phi_{k_h} = \tilde{\phi}_{\bar{k}_l}^\dagger \phi_{\bar{k}_h} = \delta_{lh}, \quad (2.12)$$

from which follows the completeness conditions

$$\sum_{l=1}^M \phi_{k_l} \tilde{\phi}_{k_l}^\dagger = \sum_{l=1}^M \phi_{\bar{k}_l} \tilde{\phi}_{\bar{k}_l}^\dagger = \mathcal{I}. \quad (2.13)$$

Equation (2.10) shows the retarded Green function for a doubly infinite system. For a semi-infinite lead, this must be modified to satisfy the boundary conditions at the end of the

leads. Consider first the left lead, which extends to $z = -\infty$ and terminates at $z = z_0 - 1$, such that the position of the first missing slice is $z = z_0$. To satisfy the boundary condition that the Green function must vanish at $z = z_0$, we subtract from the right hand side of (2.10) a wavefunction of the form

$$\Delta_z(z', z_0) = \sum_{lh}^M \phi_{\bar{k}_h} e^{i\bar{k}_h z} \Delta_{hl}(z', z_0), \quad (2.14)$$

where $\Delta_{hl}(z', z_0)$ is a complex matrix, determined from the condition that the Green function vanishes at z_0 , which yields

$$\begin{aligned} \Delta_z(z', z_0) = \Delta_{z'}(z, z_0) = \\ \sum_{l,h=1}^M \phi_{\bar{k}_h} e^{i\bar{k}_h(z-z_0)} \tilde{\phi}_{\bar{k}_h}^\dagger \phi_{k_l} e^{ik_l(z_0-z')} \tilde{\phi}_{k_l}^\dagger \mathcal{V}^{-1}, \end{aligned} \quad (2.15)$$

For the purpose of computing the scattering matrix, we shall require the Green function of the semi-infinite left-lead $\tilde{g}_{zz'}(z_0) = g_{zz'} - \Delta_z(z', z_0)$ evaluated on the surface of the lead, namely at $z = z' = z_0 - 1$. Note that in contrast with the Green's function of a doubly infinite lead, which depends only on the difference between z and z' , the Green's function \tilde{g} of a semi-infinite lead for arbitrary z, z' is also a function of the position z_0 of the first missing slice beyond the termination point of the lead. Writing $g_L = g_{(z_0-1)(z_0-1)}(z_0)$ yields for this surface Green function

$$g_L = \left[\mathcal{I} - \sum_{l,h} \phi_{\bar{k}_h} e^{-i\bar{k}_h} \tilde{\phi}_{\bar{k}_h}^\dagger \phi_{k_l} e^{ik_l} \tilde{\phi}_{k_l}^\dagger \right] \mathcal{V}^{-1}. \quad (2.16)$$

Similarly on the surface of the right lead, which extends to $z = +\infty$, the corresponding surface Green function is

$$g_R = \left[\mathcal{I} - \sum_{l,h} \phi_{k_h} e^{ik_h} \tilde{\phi}_{k_h}^\dagger \phi_{\bar{k}_l} e^{-i\bar{k}_l} \tilde{\phi}_{\bar{k}_l}^\dagger \right] \mathcal{V}^{-1}, \quad (2.17)$$

The expressions (2.16) and (2.17), when used in conjunction with (2.8) form a versatile method of determining lead Green functions, without the need to perform k-space integrals

or a contour integration. As a consequence of translational invariance of the doubly infinite system, the surface Green functions are independent of the position of the surface z_0 . Furthermore as noted below, in the case of different vectors ϕ_k corresponding to the same real k -vector k , the current operator is not diagonal. Hence it is convenient to perform a unitary rotation in such degenerate sub-space to ensure the unitarity of the S-matrix.

B. The effective Hamiltonian of the scattering region.

Given the Hamiltonian of a scattering region and a matrix of couplings to the surfaces of external leads, the Green function of the scatterer plus leads can be computed via Dyson's equation. For structures of the form of Fig 1, which possess a quasi-one dimensional geometry and a Hamiltonian which is block tri-diagonal, this task can be made more efficient by first projecting out the internal degrees of freedom of the scatterer, to yield an effective Hamiltonian involving only those degrees of freedom on the surfaces of the external leads. In the literature, depending on the context or details of implementation, this procedure is sometimes referred to as “the recursive Green function technique” or “the decimation method”, but is no more than an efficient implementation of Gaussian elimination.

Consider a scatterer composed on $N - 2M$ degrees of freedom. Then the Hamiltonian for the scatter plus semi-infinite leads is of the form $H = H_L + H_R + \tilde{H}$, where H_L, H_R are the Hamiltonians of the left and right isolated leads and \tilde{H} a $N \times N$ Hamiltonian describing the scattering region and any additional couplings involving surface sites of the leads induced by the presence of the scatterer. The aim of the decimation (i.e. recursive Green function) method is to successively eliminate the internal degrees of freedom of the scatterer, which we label $i, i = 1, 2, \dots, N - 2M$, to yield a $(2M) \times (2M)$ effective Hamiltonian H_{eff} . After eliminating the degree of freedom $i = 1$, \tilde{H} is reduced to a $(N - 1) \times (N - 1)$ matrix with elements

$$H_{ij}^{(1)} = \tilde{H}_{ij} + \frac{\tilde{H}_{i1}\tilde{H}_{1j}}{E - \tilde{H}_{11}} \quad (2.18)$$

Repeating this procedure l times we obtain the “decimated” Hamiltonian at l -th order

$$H_{ij}^{(l)} = H_{ij}^{(l-1)} + \frac{H_{il}^{(l-1)} H_{lj}^{(l-1)}}{E - H_l^{(l-1)}}, \quad (2.19)$$

and after $N - 2M$ such steps, an effective Hamiltonian $H_{\text{eff}} = H^{N-2M}$ of the form

$$H_{\text{eff}}(E) = \begin{pmatrix} H_{\text{L}}^*(E) & H_{\text{LR}}^*(E) \\ H_{\text{RL}}^*(E) & H_{\text{R}}^*(E) \end{pmatrix}, \quad (2.20)$$

In this expression, $H_{\text{L}}^*(E)$ ($H_{\text{R}}^*(E)$) describes intra-surface couplings involving degrees of freedom belonging to the surface of the left (right) lead and $H_{\text{LR}}^*(E) = H_{\text{LR}}^*(E)^\dagger$ describes the effective coupling between the surfaces of the left and the right leads.

Since the effective Hamiltonian is energy dependent, this procedure is particularly useful method when we wish to compute the Green function at a given energy. It is also very efficient in the presence of short range interactions, because only matrix elements involving degrees of freedom coupled to the decimated one, are redefined. Since the problem now involves only $(2M) \times (2M)$ matrices, it is straightforward to obtain the surface Green function for the whole system (i.e. the scattering region attached to semi-infinite leads) by solving Dyson's equation

$$G(E) = (g(E)^{-1} - H_{\text{eff}}(E))^{-1}, \quad (2.21)$$

where

$$g(E) = \begin{pmatrix} g_{\text{L}}(E) & 0 \\ 0 & g_{\text{R}}(E) \end{pmatrix}, \quad (2.22)$$

with g_{L} and g_{R} given by equations (2.16) and (2.17).

C. The scattering matrix and transport coefficients

To extract transport coefficients from the Green function, we generalize the method described in [12] (in particular see A.26 of [12]) to the case of non-orthogonal scattering channels. For a system of Hamiltonian H , the S matrix is defined to connect incoming to outgoing propagating states in the external leads. If k , (k') are real incoming (outgoing)

wavevectors of energy E , then an incident plane-wave in one of the leads, with longitudinal wavevector k , will scatter into outgoing plane-waves k' with amplitudes $s_{k'k}(E, H)$. If all plane-waves are normalized to unit flux, (by dividing by the square-root of their group velocities) then provided the plane-wave basis diagonalizes the current operator in the leads, the outgoing flux along channel k' is $|s_{k'k}(E, H)|^2$ and S will be unitary. If H is real, then S will be symmetric, but more generally time reversal symmetry implies $s_{k'k}(E, H) = s_{kk'}(E, H^*)$. For convenience, if k, k' belong to the left (right) lead, then we define reflection coefficients via $r_{k'k} = s_{k'k}$ ($r'_{k'k} = s_{k'k}$), whereas if k, k' belong to left and right leads respectively (right and left leads respectively) we define transmission coefficients $t_{k'k} = s_{k'k}$ ($t'_{k'k} = s_{k'k}$).

To extract transport properties for the system of Fig.2, consider the probability current for an electron in the Bloch state (2.3)

$$J_k = n_{k_\perp} v_{k_\perp} , \quad (2.23)$$

where n_{k_\perp} is the probability of finding an electron in a slice and v_{k_\perp} is the corresponding group velocity. It follows that the vector

$$\psi_z = \frac{1}{\sqrt{v_k}} e^{ikz} \phi_k , \quad (2.24)$$

is normalized to unit flux. To compute the group velocity we note that if $|\psi_k\rangle$ is an eigenstate (2.1), whose projection onto slice z is ψ_z , then

$$\begin{aligned} v_k &= \frac{1}{\hbar} \frac{\partial}{\partial k} \langle \psi_k | H | \psi_k \rangle = \\ &= \frac{1}{\hbar} \frac{\partial}{\partial k} \left[\phi_k^\dagger \left(H_0 + H_1 e^{ik} + H_{-1} e^{-ik} \right) \phi_k \right] = \end{aligned} \quad (2.25)$$

$$= \frac{i}{\hbar} \phi_k^\dagger \left(H_1 e^{ik} - H_{-1} e^{-ik} \right) \phi_k , \quad (2.26)$$

where the last step follows from equation (2.4) and normalization of ϕ_k .

It can be shown that the states (2.24) diagonalize the current operator only if they correspond to distinct k values. In the case of degenerate k 's, the current is in general non-diagonal. Nevertheless it is always possible to define a rotation in the degenerate subspace for which the current operator is diagonal and in what follows, when a degeneracy is encountered, we assume that such a rotation has been performed. With this convention, the current carried by a state of the form

$$\psi_z = \sum_l a_l \frac{e^{ik_l z}}{\sqrt{v_l}} \phi_{k_l}, \quad (2.27)$$

is simply $\sum_l |a_l|^2$.

It is now straightforward to generalize the analysis of [12] to the case of non-orthogonal scattering channels. Consider first a doubly infinite periodic structure, whose Green function is given by equation (2.10). For $z \geq z'$, acting on $g_{zz'}$ from the right with the following projector

$$P_l(z') = \mathcal{V} \phi_{k_l} \frac{e^{ik_l z'}}{\sqrt{v_l}}, \quad (2.28)$$

yields the normalized plane-wave (2.24). Similarly by acting on the Green function $g_{zz'}(z_0)$ of a semi-infinite left-lead terminating at z_0 , one obtains for $z \geq z'$, $z_0 \geq z$, an eigenstate of a semi-infinite lead arising from a normalized incident wave along channel k_l .

Thus the operator $P_l(z')$ and its left-going counterpart $\bar{P}_l(z')$ allow us to project-out wavefunctions from the Green function of a given structure. For example if $G_{zz'}$ is the retarded Green function for a scattering region sandwiched between two perfect leads whose surfaces are located at the points $z = 0$ and $z = L$, then for $z' \leq 0$, the projected wavefunction is of the form

$$\psi_z = \begin{cases} \frac{e^{ik_l z}}{\sqrt{v_l}} \phi_{k_l} + \sum_h \frac{r_{hl}}{\sqrt{v_h}} e^{i\bar{k}_h z} \phi_{\bar{k}_h} & z \leq 0 \\ \sum_h \frac{t_{hl}}{\sqrt{v_h}} e^{ik_h z} \phi_{k_h} & z \geq L \end{cases}, \quad (2.29)$$

where $r_{hl} = r_{\bar{k}_h, k_l}$, $t_{hl} = t_{k_h, k_l}$ are reflection and transmission coefficients associated with an incoming state from the left. In particular for $z = L$, $z' = 0$, one obtains

$$\sum_h \frac{t_{hl}}{\sqrt{v_h}} e^{ik_h L} \phi_{k_h} = G_{L0} P_l(0), \quad (2.30)$$

and hence

$$t_{hl} = \tilde{\phi}_{k_h}^\dagger G_{L0} \mathcal{V} \phi_{k_l} \sqrt{\frac{v_h}{v_l}} e^{-ik_h L}. \quad (2.31)$$

Since the right hand side of (2.31) involves only the surface Green function of equation (2.21) the transmission coefficients (and by analogy all other transport coefficients) are determined. Since the above analysis is valid for any choice of the Hamiltonians H_0 and H_1 , this approach is very general.

III. RESULTS FOR CO AND NI BASED MULTILAYERS

Using the technique developed above, we have studied transport properties of multilayers formed from Co and Ni as magnetic materials and several $3d$, $4d$ and $5d$ transition metals as non-magnetic materials. All of these metals possess an fcc lattice structure with the following lattice constants (Tab.I).

It is clear that Co and Ni have a good lattice match with Cu, while for the other metals the lattice mismatch is large and may introduce distortion and defects at the interface. The latter introduces an additional scattering at the interfaces, but is neglected in our calculations. Nevertheless we will show that large values of the GMR ratio can be obtained, in agreement with the largest experimental values, which suggests that CPP GMR is a bulk effect, whose main features are contained in a ballistic quantum description of the conductance with an accurate band structure. In what follows we model all the metals by an *spd* tight-binding Hamiltonian with nearest neighbor couplings, whose parameters are chosen to fit the band structure evaluated from first principle calculations [13]. The hopping parameters at the heterojunctions between different materials are assigned the geometric mean of the pure metal values.

A. The DOS and Conductance of the pure metals

We begin our analysis by examining the DOS and conductance of the pure metals. Since the Hamiltonians include spd hybridization, angular momentum states are not eigenstates of the system. Nevertheless to understand the relative rôle of the angular momentum inter-band and intra-band scattering, it is useful to project the DOS and conductance onto an angular momentum basis. We will label as an s -like electron (and similarly for the p and d electrons) an electron whose s -component $|\langle s|\psi\rangle|^2$ of the wave function $|\psi\rangle$ is much larger than the p and d components.

The DOS's for the two spin sub-bands of Co and Ni are very similar and as an example the Co DOS is shown in Fig.3.

As in all the d transition metals, the DOS is formed from a localized d band embedded in parabolic s and p bands. The broadening of the bands is roughly the same in Co and Ni, as well as the position of the majority band with respect to the Fermi energy. In both materials, the Fermi energy lies just above the edge of the majority d band, while the minority band is obtained from a rigid shift of the majority band toward higher energies, the magnitude of which is larger in Co than in Ni. In both the minority bands of Co and Ni the Fermi energy lies well within the d band and the DOS is completely dominated by the d electrons. A rough estimate of the mismatch between the minority d bands of Co and Ni can be obtained from the on-site energies of the d electrons in the minority band. As shown in table II, the difference between the on-site energies of the d minority electrons in Co and Ni is about 0.7eV and corresponds to the relative shift of the bands (the on-site energies shown in the table are chosen in order to have the Fermi energy $E_F = 0$).

The conductance of pure Co and Ni is determined solely by the DOS. For majority electrons at the Fermi energy, the current is carried by the s , p and d electrons, which give almost equal contributions. On the other hand the current carried by minority electrons is completely dominated by the d electrons, with the contributions from s and p electrons being no larger than 10%. If we neglect the relative shift in energies of the minority bands,

the Ni and Co conductances possess the same qualitative features and since the effective mass is proportional to the inverse of the band width, we find that the current carried by majority electrons is formed from a mixture of light s and p electrons and heavy d electrons, whereas the minority-electron current is carried almost entirely by heavy d electrons.

Now consider the non-magnetic $3d$, $4d$ and $5d$ transition metals with fcc lattices. A glance at the DOS of these materials reveals three types of band structure: i) the DOS closely matches the DOS of the majority spin sub-band of Co and Ni (e.g. Cu and Au), ii) the DOS has only sp components at the Fermi energy, with the d component highly suppressed (as in Ag), iii) the DOS is composed of an almost pure d component at the Fermi energy (e.g. for Pd and Pt). Examples of each of these are given in figure 4, which shows the DOS of Cu, Ag and Pd and in figure 5, which shows the corresponding conductances.

In what follows, we shall show that for ballistic structures, the mismatch between the bands of the magnetic and non-magnetic metals forming the multilayer is the key feature which determines the conductance. Moreover, although the positions of the s and p bands are the same for both spins, for d -electrons the two spin sub-bands possess a different mismatch at the interface and therefore this mismatch (potential step for d electrons at the interface) largely determines the magnitude of CPP GMR.

In addition to the above generic features, the on-site energies of the s bands of Au and Pt are small compared with those of Ni and Co. In the Co/Au and Co/Pt multilayers, this may induce strong scattering of the s -electrons, resulting in a strong suppression of the s -electron contribution to the total conductance. This effect should be weaker in the Pt-based than in the Au-based multilayers, because DOS of Platinum has mainly a d character at the Fermi energy, which means that the Co/Pt multilayers will feel the effect of the large s -band mismatch only through the hybridization of the s and d bands at the Fermi energy.

Figure 5 shows how these three distinct DOS characteristics are reflected in the conductances of the normal metals and give rise to three different scenarios for charge transport: i) the contributions to the current from s , p and d electrons are almost equal (e.g. in Cu and Au), ii) the current has a strong sp character (e.g. in Ag), iii) the current has a strong

d character (e.g. Pd and Pt).

These different characteristics of the current carriers in the non-magnetic metals give rise to another important source of interface scattering. Since the majority spins in the magnetic metals are mainly *sp* electrons with light effective masses and the minority spins are *d* electrons with heavy effective masses, it is clear that depending on the choice of non-magnetic metal, different spin-dependent inter-band scattering must occur at the interfaces. For example in the Co/Ag system, a majority spin propagates in Co as a mixture of *s*, *p* and *d* electrons and in Ag as an *sp* electron. This means that an electron in the Ag, whose spin is in the same direction of the magnetization, can enter Co as an *sp* electron without the need for strong inter-band scattering. On the other hand if its spin points in the opposite direction, it will undergo inter-band scattering, because in the minority band the electron must propagate as a *d* electron. Moreover the inter-band scattering involves final states with a large DOS, and hence a scattering is expected to be strong.

The above observations suggest that the key mechanisms affecting transport are i) a strong band mismatch and ii) a strong inter-band scattering. The best GMR multilayers must be able to maximize electron propagation in one of the two spin bands and to minimize it in the other. To achieve this result the high conduction spin band should have a small band mismatch and weak inter-band scattering at the heterojunctions, while the low conduction band should have a large band mismatch and strong inter-band scattering.

B. A comparison between Co-based and Ni-based multilayers.

To clarify how the spin polarization of the magnetic material affects the properties of the GMR multilayers, we begin by examining GMR in Cu-based multilayers, in which the magnetic metals are either Ni or Co. All the multilayers consist of ten bilayers of the form A/Cu where A is Co or Ni, attached to two semi-infinite Cu leads. After calculating the different spin conductances in the ferromagnetic and antiferromagnetic configurations, the GMR ratio is obtained from equation (1.1). In all our calculations the current flows in the

(110) crystalline direction and the structures are translationally invariant within the layers. In what follows we consider 8100 k_{\parallel} points (90×90) in the plane of the layers. We have estimated that the GMR ratio calculated with 2×10^4 k_{\parallel} points on average differs by $\sim 3\%$, from that calculated using 8100 k_{\parallel} points ($\frac{\text{GMR}(8100) - \text{GMR}(2 \times 10^4)}{\text{GMR}(8100)} \sim 3\%$). Since the oscillations of the GMR ratio with respect to the layer thicknesses are larger than 3%, the choice of 8100 k_{\parallel} points allows us to investigate the oscillating behavior of the conductance and the GMR, and is a good compromise between the accuracy of the calculation and the required computer time.

Initially we fix the magnetic layer thickness to 5 atomic planes (AP), and calculate the conductance and GMR as a function of the Cu layer thickness. In what follows, we normalize the conductance by dividing by the conductance of a single spin in the pure metallic leads (hence in this case by one half of the total Cu conductance, because of spin degeneracy), to yield the results shown in figure 6.

From figure 6 it is clear that the Co based multilayers possess larger GMR ratios. In the ferromagnetic configuration, the majority electrons possess high conductances in both cases, reflecting the good match between the majority bands of Co and Ni, and the Cu band. Moreover the better match of the s and p majority bands of Ni with Cu, compared with those of Co, gives rise to a slightly higher conductance in majority channel for Ni than for Co. A similar argument explains the difference in the conductances of the minority channel. As we can see from table II, the minority d band of Ni is a better match to Cu than that of Co, as indicated by the difference in the on-site energies about 0.7 eV. Hence for the minority band, the interface scattering between Co/Cu is greater for Ni/Cu. In the antiferromagnetic configuration, both spins undergo the same scattering sequence, belonging alternately to the majority and to the minority bands. The total spin conductance in the antiferromagnetic configuration is found to be close to that of the minority band in the ferromagnetic configuration, because the minority band mismatch is larger than the majority band, and dominates the scattering.

The ratio R between the conductance (Γ) of the AF configuration and of the minority

band in the F configuration ($R = \Gamma(\text{AF})/\Gamma(\text{F minority})$) is ~ 0.6 for Co/Cu and ~ 0.9 for Ni/Cu. This difference can be understood by modeling the interface scattering through an effective step potential, whose magnitude is equal to the band mismatch, as will be discussed in a future publication. The effective scattering potential in the antiferromagnetic configuration will be a sequence of high steps (minority band) and low steps (majority band). The calculated R ratios arise, because the perturbation of the minority steps due to the majority steps, is smaller in Ni/Cu than in Co/Cu. From this analysis the splitting between the two spin sub-bands in the magnetic materials is the crucial parameter leading to large GMR ratios and since such splitting is larger in Co than in Ni, Co emerges as a natural candidate for high GMR ratio multilayers. Note that highest possible values of GMR can probably be achieved with the use of half-metallic ferromagnets with 100% spin polarization of electrons [19].

Having examined the dependence of transport properties on the normal-metal layer thickness, we now examine the dependence on the magnetic-layer thickness. For a fixed Cu layer-thickness of 5 atomic planes, figure 7 shows results for Co/Cu and Ni/Cu multilayers.

A key result of this figure is that for thin magnetic layers, GMR in both Ni/Cu and Co/Cu multilayers is suppressed due to tunneling through the effective potential barrier. Thus we predict a lower limit of approximately 4 atomic planes to the magnetic-layer thickness, in order to achieve the highest possible GMR ratio. In what follows we will only consider thicknesses larger than this value.

C. Dependence of GMR on non-magnetic spacer material.

We now consider the dependence of GMR on the choice of non-magnetic material in Co and Ni-based multilayers. In all calculations we fix the Co thickness at 5 and 10 atomic planes and vary the thickness of the non-magnetic layers from 1 to 40 atomic planes. The material in the external leads is the same non-magnetic material used for the multilayers (e.g. Ag in Co/Ag multilayers). Table III shows the average value of the GMR ratio and the root

mean square amplitude of oscillation around such value (Δ). To highlight the fact that GMR is an oscillatory function of the normal-metal thickness with an amplitude which decreases with increasing thickness, the table also shows the mean square oscillation calculated for non-magnetic metal layers thicknesses between 1-10 ($\Delta 1$). In the table the subscript at Co indicates the number of atomic planes of the Co layers. The penultimate row of the table shows results for the Ni/Cu system, for which we believe that no CPP experimental results are currently available, even though the CIP conductance in high magnetic field has been studied [14]. We also speculate on the possibility of using Co/Ni [15,16] as a GMR material, results for which are shown on the last row.

From the Table III it is clear that the GMR ratio results to depend quite sensitively on the multilayer geometry, i.e. on the layer thicknesses. In fact the simulations with the Co thickness fixed at 5 atomic planes seem to suggest that the *sp* conductors as spacer layers (Cu, Ag) result in larger GMR ratios in this case. The simulations with 10 Co atomic planes show that the multilayers with *d*-electron spacers (Pd, Pt) correspond to relatively larger GMR. Nevertheless it is clear that the Co based multilayers present much larger GMR ratios than the Ni based multilayers. The table also demonstrates that the conductors dominated by *d* electrons, namely Pd and Pt, possess very similar GMR ratios and amplitudes of oscillation and that Au possesses the largest amplitude oscillations. As examples, figure 8 shows plots of the GMR ratio as a function of the non-magnetic metal layer thickness for the Co/Ag and Co/Pd systems.

In all cases (excluding Au) the oscillations are small compared with the average value of the GMR ratio, suggesting that there is an additional contribution to the long range oscillations observed experimentally. This is most likely to arise from a periodic deviation from a perfect antiferromagnetic configuration, the possibility of which is neglected in our calculations. It is important to point out that perfect antiferromagnetic alignment of the multilayer in zero magnetic field is a consequence of the exchange coupling of the adjacent magnetic layers through the non-magnetic layer. The strength and phase of such coupling depend critically on the Fermi surface of the non-magnetic metal [17]. To the best of our

knowledge no experimental data are available for the d conductor multilayers, for which the antiferromagnetic configuration may not be achievable. Nevertheless, in spin valve systems such an antiferromagnetic configuration can be always obtained by tuning the coercive fields of the different magnetic layers, for instance by an appropriate choice of the spin valve geometry, or by using some magnetization pinning technique. Hence our theoretical predictions on Co/Pd and Co/Pt multilayers can, in principle, be tested in the spin valves.

The above results for the GMR ratio hide the material dependence of the electrical conductance and with a view to comparing these with their band structures, we now present results for the conductances of the different spin channels and of the AF configuration. In the tables IV, V and VI we present the conductance (Γ), the mean conductance oscillation ($\Delta\Gamma$), their ratio ($\Delta\Gamma/\Gamma$), the maximum of the conductance oscillations ($\Delta\Gamma_{\max}$) and its ratio with the mean conductance ($\Delta\Gamma_{\max}/\Gamma$), respectively for the majority electrons in the ferromagnetic configuration, the minority electrons in the ferromagnetic configuration, and both spins in the antiferromagnetic configuration. All conductances are normalized to the single-spin conductance of the non-magnetic-metal leads.

The Tables IV-VI illustrate that, with the exception of Au, materials belonging to the same class have similar normalized conductances. For Cu and Ag the majority (minority) band is a high (low) transmission band, leading to a large GMR ratio for such materials. The majority bands of these two materials match that of Co and there is little interband scattering (even less in Ag where the electrons at the Fermi energy are completely sp). In contrast the minority bands are subject to a large scattering potential due to the difference between the on-site energies of the d -band, and also large interband scattering, due to the full d character of the minority d band of Co. On the other hand, for Pd and Pt, which are d conductors, both sub-bands undergo to high scattering albeit for different reasons. The on-site energies of the majority band of Co, and of Pd and Pt, are roughly the same, ensuring a good band match. Nevertheless the broadening of the d majority band of Co is associated with a mixing of s , p and d electrons, while the Pd and Pt bands are mainly d -like. Hence, in the majority band of Co/Pd and Co/Pt superlattices, large inter-band

scattering is present. In contrast the minority band is d -like in Co, Pd, and Pt, but there is a significant difference in the on-site energies, resulting in a large effective potential at the interface.

The Au/Co multilayers lie somewhat outside the above picture, because even though the d band resembles that of Ag, the on-site energies of the s and p bands are considerably smaller than the corresponding bands in Co. This means that strong scattering occurs in the s and p bands and since the s and p electrons of Au carry most of the current, there is a strong suppression of the conductance in all spin channels. From the above tables, we see that the Co/Au system possesses a low conductance in all the spin channels and in the antiferromagnetic configuration.

Finally we note that compared with the majority spin channel the oscillations are larger in the minority spin channel and in the antiferromagnetic configuration. This suppression of oscillations in the former occurs because of the better band matching in the majority band. In figure 9 we show the conductance of the minority band as a function of the non-magnetic layers thickness, for all the materials studied.

The oscillations that we observe never exceed 20% of their mean value (except for the Co/Au system) and they are larger for smaller thicknesses. This is substantially smaller than the observed values for Co/Ni system [15,16]. The difference may in part be related to scattering on disorder, always present in experimental systems, and to simplicity of a tight-binding model that we used. In addition, actual magnetic configuration in those systems can be somewhat different as compared to an ideal one that we considered. It is interesting to note that, generally, materials with small conductances ($\Gamma < 0.25$ using the usual normalization for conductances) possess larger oscillations, because low conductances indicate strong scattering potentials, and hence larger fluctuations. A qualitative picture of these conductance oscillations will be presented in a future publication, [18] where the above quantitative results are compared with a simple Kronig-Penney model.

IV. CONCLUSION

Firstly, we have developed a completely general Green's function technique for elastic spin-dependent transport calculations, which (i) scales linearly with a system size and (ii) allows straightforward application to general tight-binding (*spd* in the present work) Hamiltonians. This technique can be applied to unrestricted studies of different systems, including tunneling spin valves [19,20] and magnetic multilayers with superconducting leads. The formulae (2.16) and (2.17) for the surface Green functions of external leads are the central result of the first part. Explicit general expressions for the Green's functions enable us to avoid using a small imaginary part in energy.

Secondly, we have presented an extensive study of transport in magnetic multilayers in CPP (current perpendicular to planes) geometry in the limit of large coherence length. Ni and Co were considered as materials for magnetic layers and several *3d*, *4d* and *5d* metals as non-magnetic spacers. Key parameters have been identified as controlling a giant magnetoresistance in those systems. These are the character of electronic states at the Fermi level and a mismatch in relevant band edges across interfaces. We have found that, in accordance with experiment [15,16], there are oscillations in the conductance as a function of both magnetic and spacer layer thicknesses. The magnitude of the calculated oscillations is, however, smaller than observed experimentally. Some reasons for this behavior have been indicated and deserve further study. A semi-quantitative analysis of the oscillations will be presented elsewhere [18].

V. ACKNOWLEDGEMENTS

The authors wish to acknowledge Prof. Ivan Schuller for valuable and useful discussions. This work is supported by the EPSRC and the EU TMR Programme.

- [1] M.N.Baibich, J.M.Broto, A.Fert, F.Nguyen Van Dau, F.Petroff, P.Etienne, G.Creuzet, A.Friederich, and J.Chazelas, Phys. Rev. Lett. **61**, 2472 (1988); G.Binasch, P.Grünberg, F.Sauerbach and W.Zinn, Phys. Rev. **B 39**, 4828 (1989)
- [2] R.E.Camley and J.Barnas, Phys. Rev. Lett. **63**, 664 (1989)
- [3] W.P.Pratt Jr., S.-F.Lee, J.M.Slaughter, R.Loloee, P.A.Schroeder, J.Bass, Phys. Rev. Lett. **66**, 3060 (1991); M.A.M.Gijs, S.K.J.Lenczowski, J.B.Giesbers, Phys. Rev. Lett. **70**, 3343 (1993)
- [4] N.F. Mott, Adv. Phys. **13**, 325 (1964).
- [5] S.S.P.Parkin, Phys. Rev. Lett. **67**, 3598 (1991)
- [6] K.M.Schep, P.J.Kelly, and G.E.W.Bauer, Phys. Rev. Lett. **74**, 586 (1995)
- [7] K.M.Schep, P.J.Kelly, and G.E.W.Bauer, Phys. Rev. **B 57**, 8907 (1998) and references therein.
- [8] M.Büttiker, Y.Imry, R.Landauer, S.Pinhas, Phys. Rev. **B 31**, 6207 (1985)
- [9] M.A.M.Gijs, G.E.W.Bauer, Adv. Phys., **46**, 285 (1997)
- [10] W.H. Butler, X.G. Zhang, D.M.C. Nicholson, and J.M. MacLaren, Phys. Rev. B **52**, 13399 (1995); M.D. Stiles, J. Appl. Phys. **79**, 5805 (1996); E.Yu.Tsymbal, D.G.Pettifor, Phys. Rev. **B 54**, 15314 (1996).
- [11] J.Mathon, Phys. Rev. **B 55**, 960 (1997).
- [12] C.J.Lambert, V.C.Hui, and S.J.Robinson, J. Phys.: Condens. Matter, **5**, 4187 (1993)
- [13] D.A.Papaconstantopoulos, *Handbook of the Band Structure of Elemental Solids*, (Plenum, New York, 1986)
- [14] H.Sato, T.Matsudai, W.Abdul-Razzaq, C.Fierz, P.A.Schroeder, J. Phys.: Condens. Matter, **6**, 6151 (1994)
- [15] J.M.Gallego, D.Lederman, S.Kim, I.K.Schuller Phys. Rev. Lett. **74**, 4515 (1995)

- [16] D.Lederman, J.M.Gallego, S.Kim, I.K.Schuller *J.Magn. Magn. Mater* **183**, 261 (1998)
- [17] P.Bruno, *Phys. Rev. B* **52**, 411 (1995)
- [18] S.Sanvito, C.J.Lambert, J.H.Jefferson, A.M.Bratkovsky, to be published
- [19] A.M.Bratkovsky, *Phys. Rev. B* **56**, 2344 (1997)
- [20] A.M.Bratkovsky, *Appl. Phys. Lett.* **72**, 2334 (1998)

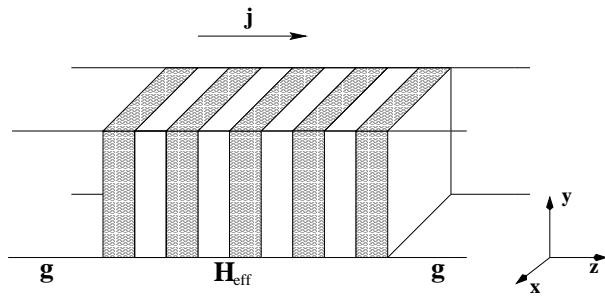


FIG. 1. Sketch of a finite superlattice connected to two semi-infinite leads.

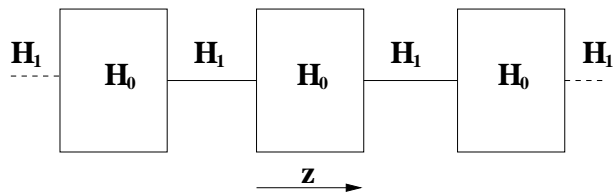


FIG. 2. A doubly infinite system formed from periodically repeated slices.

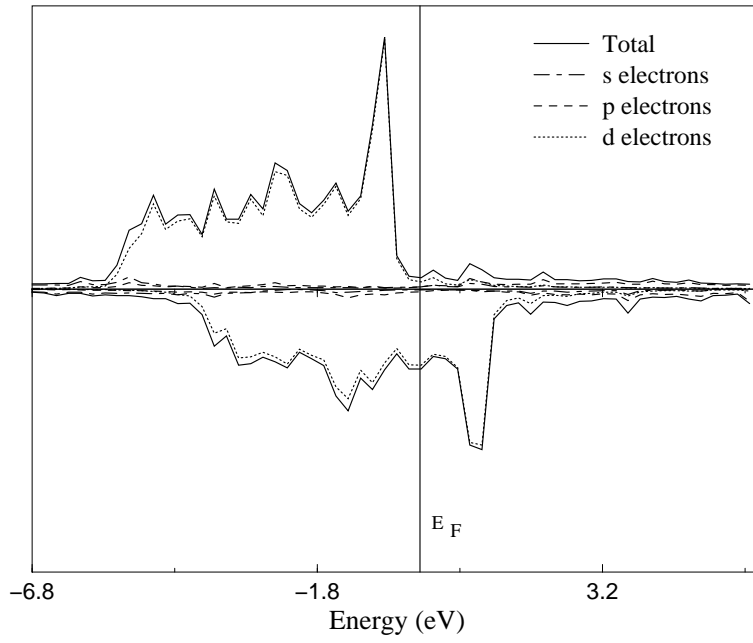


FIG. 3. DOS for pure Co. The vertical line denotes the position of E_F that is chosen to be 0 eV.

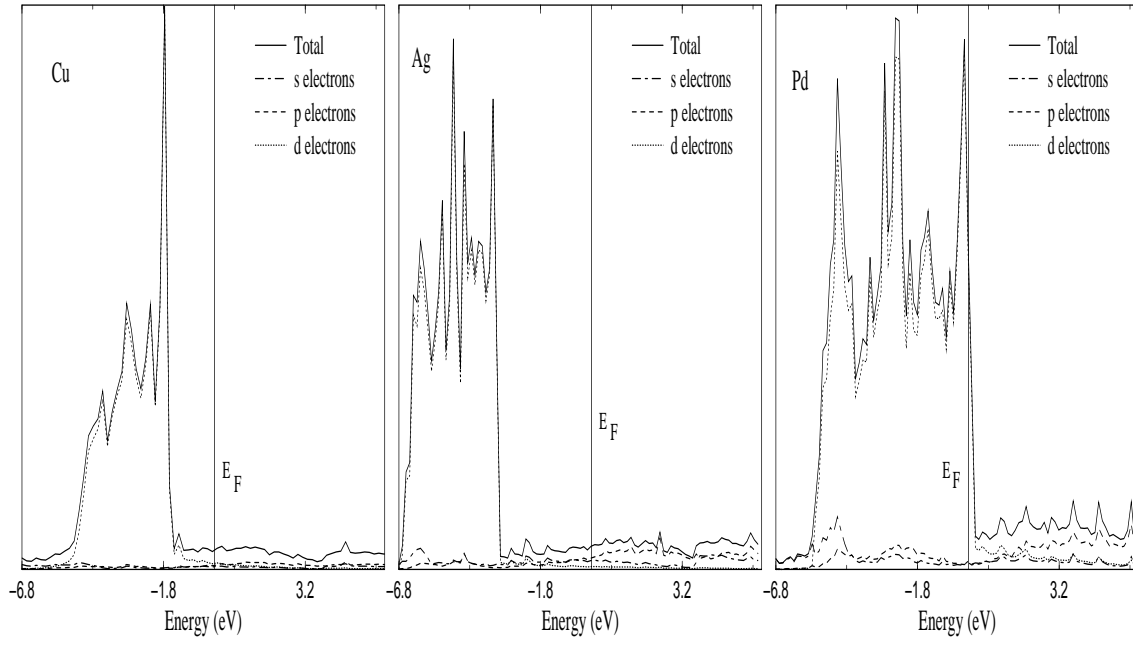


FIG. 4. DOS for pure Cu, Ag and Pd. The vertical lines denote the position of the Fermi energy, which is chosen to be $E_F = 0$

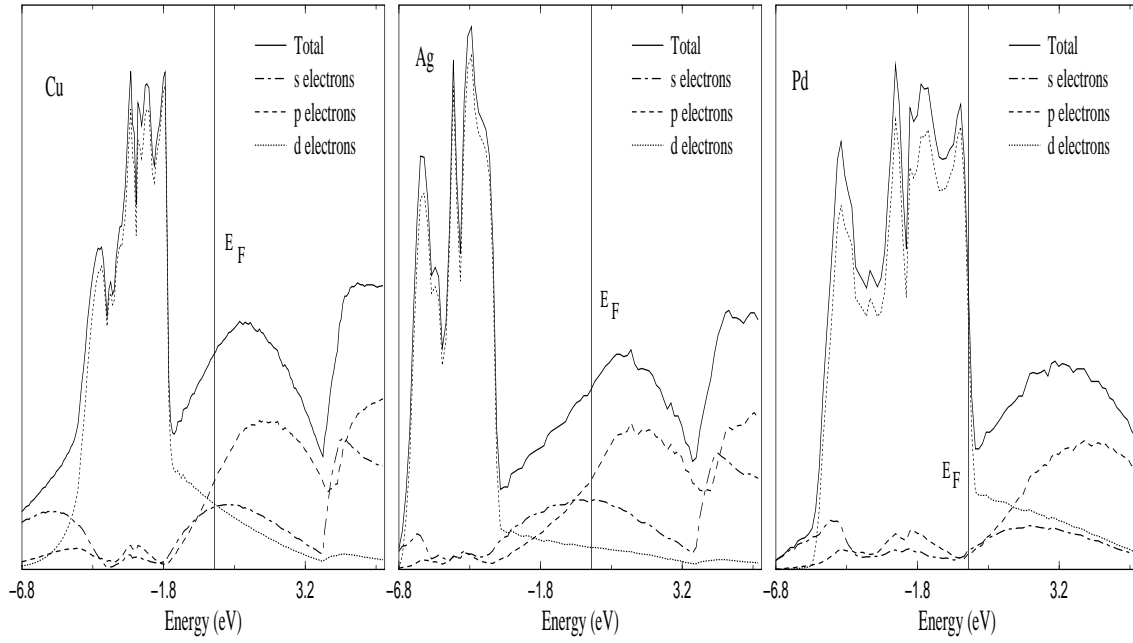


FIG. 5. The conductance for pure Cu, Ag and Pd. The vertical lines denote the the Fermi energy, $E_F = 0$.

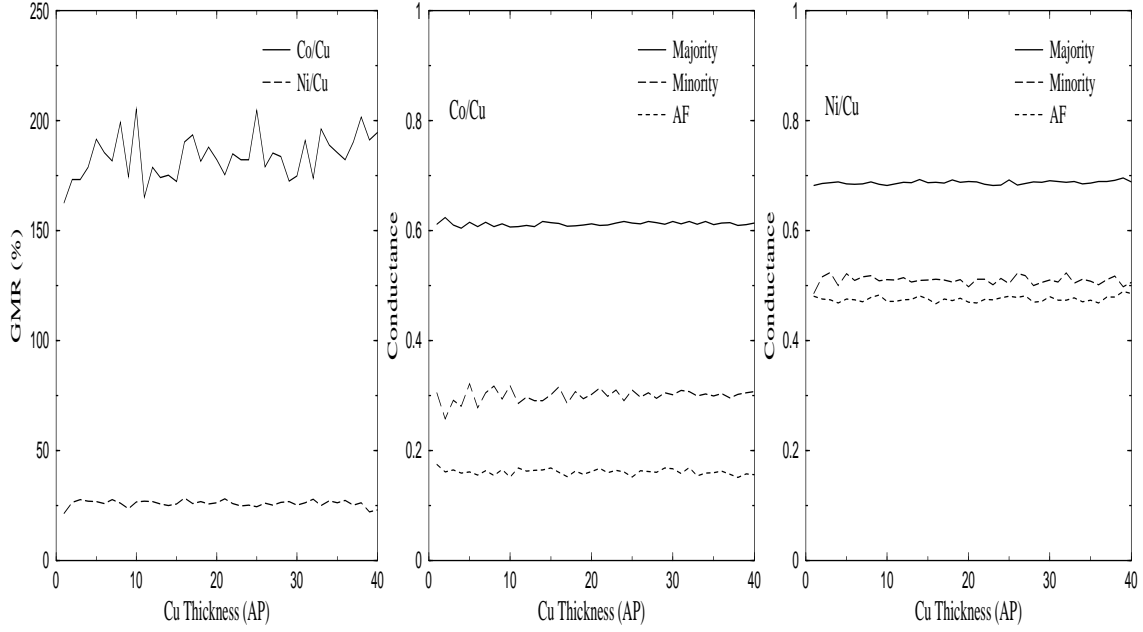


FIG. 6. GMR and spin conductance for Co/Cu and Ni/Cu systems as a function of the Cu layers thickness. The first graph is the GMR, the second is the conductance for the Co/Cu system normalized to the conductance of pure Cu and the third is the conductance of the Ni/Cu system with the same normalization

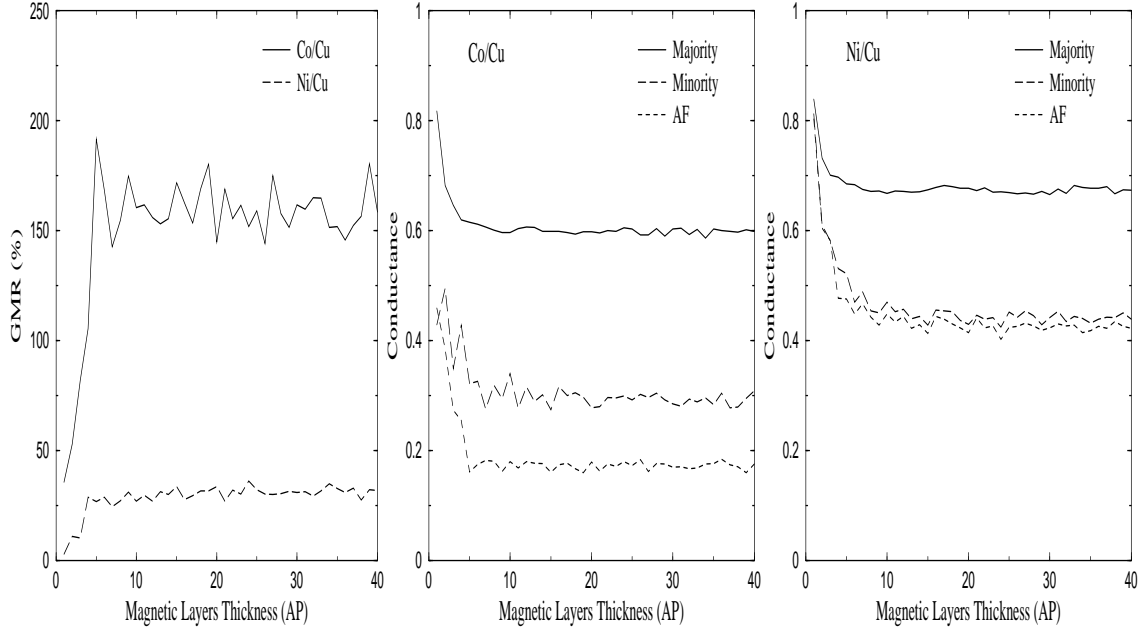


FIG. 7. GMR and spin conductance for Co/Cu and Ni/Cu systems as a function of Co and Ni layers thicknesses. The first graph is the GMR, the second is the conductance for the Co/Cu system normalized to the conductance of pure Cu and the third is the conductance of the Ni/Cu system with the same normalization.

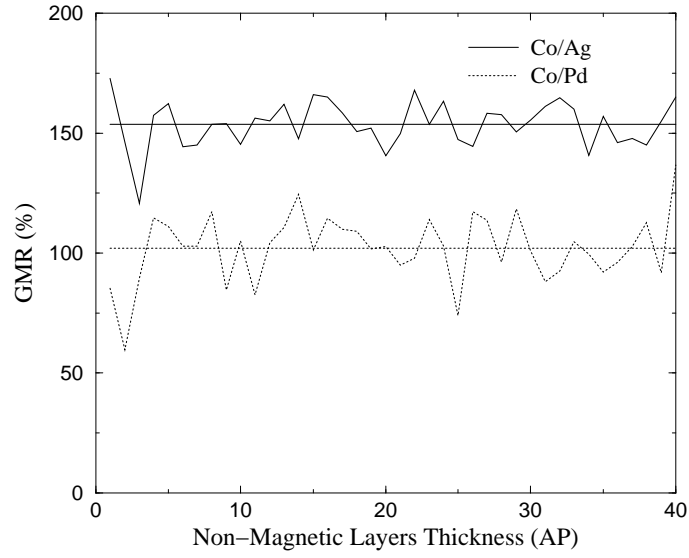


FIG. 8. GMR as a function of the non-magnetic metal layer thickness for Co/Ag and Co/Pd. The horizontal lines denote the position of the average GMR

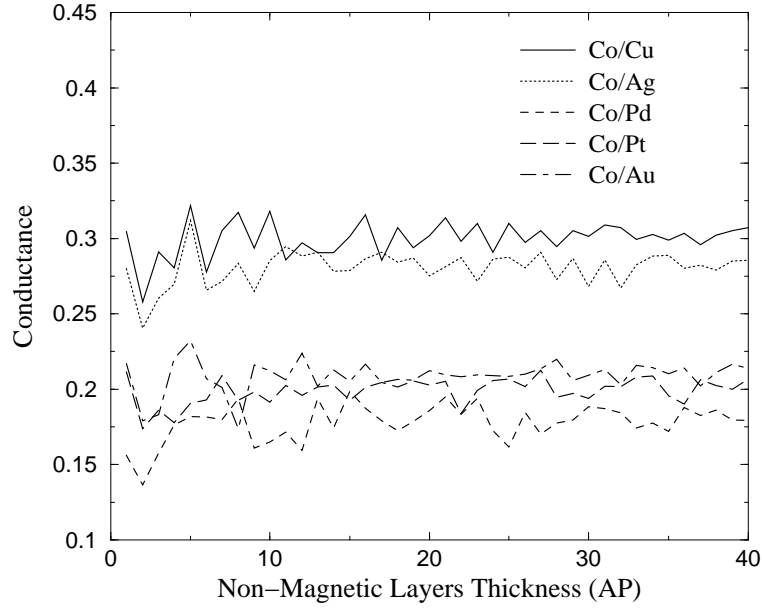


FIG. 9. Conductance of the minority spin electrons as a function of the non-magnetic layers thickness

Metal	Lattice Constant (\AA)
Co	3.55
Ni	3.52
Cu	3.61
Ag	4.09
Pd	3.89
Au	4.08
Pt	3.92

TABLE I. Lattice constants of the metals considered in the calculation

Metal	E_s (eV)	E_p (eV)	$E_{d \text{ majority}}$ (eV)	$E_{d \text{ minority}}$ (eV)
Co	5.551	14.025	-2.230	-0.660
Ni	4.735	11.850	-2.114	-1.374
Cu	2.992	10.594	-2.746	-2.746
Ag	2.986	9.127	-4.650	-4.650
Pd	5.764	11.457	-2.050	-2.050
Au	0.329	10.081	-3.823	-3.823
Pt	1.849	11.523	-2.614	-2.614

TABLE II. On-site energies used in the calculations

Multilayer	GMR ratio (%)	Δ (%)	$\Delta 1$ (%)	Δ/GMR (%)	$\Delta 1/\text{GMR}$ (%)
Co₅/Cu	183.7	10.0	12.4	5.4	6.7
Co₅/Ag	153.7	9.5	13.1	6.1	8.5
Co₅/Pd	102.0	13.9	16.7	13.7	13.4
Co₅/Pt	104.1	10.9	15.6	10.5	15.0
Co₅/Au	98.8	20.4	33.62	20.6	34.0
Co₁₀/Cu	150.7	9.2	9.2	6.1	6.1
Co₁₀/Ag	131.0	7.6	5.3	5.8	4.1
Co₁₀/Pd	165.2	31.1	32.2	18.8	19.4
Co₁₀/Pt	175.7	14.8	21.1	8.4	12.5
Co₁₀/Au	138.8	20.1	26.4	14.5	17.8
Ni₅/Cu	25.9	1.5	1.8	5.8	6.9
Ni₅/Co₅	66.1	4.1	6.6	6.2	10.0

TABLE III. GMR ratio and GMR oscillations for different metallic multilayers

Multilayer	Γ	$\Delta\Gamma$	$\Delta\Gamma/\Gamma$ (%)	$\Delta\Gamma_{\max}$	$\Delta\Gamma_{\max}/\Gamma$ (%)
Co₅/Cu	0.61	$3.76 \cdot 10^{-3}$	0.61	$1.17 \cdot 10^{-2}$	1.92
Co₅/Ag	0.66	$4.10 \cdot 10^{-3}$	0.62	$1.24 \cdot 10^{-2}$	1.88
Co₅/Pd	0.35	$5.32 \cdot 10^{-3}$	1.50	$1.52 \cdot 10^{-2}$	4.29
Co₅/Pt	0.38	$5.01 \cdot 10^{-3}$	1.31	$1.87 \cdot 10^{-2}$	4.91
Co₅/Au	0.24	$1.22 \cdot 10^{-2}$	4.94	$5.07 \cdot 10^{-2}$	20.52
Co₁₀/Cu	0.59	$5.33 \cdot 10^{-3}$	0.90	$1.06 \cdot 10^{-2}$	1.81
Co₁₀/Ag	0.63	$4.37 \cdot 10^{-3}$	0.69	$1.31 \cdot 10^{-2}$	2.06
Co₁₀/Pd	0.33	$8.89 \cdot 10^{-3}$	2.67	$2.05 \cdot 10^{-2}$	6.14
Co₁₀/Pt	0.37	$5.02 \cdot 10^{-3}$	1.37	$1.25 \cdot 10^{-2}$	3.41
Co₁₀/Au	0.24	$1.05 \cdot 10^{-2}$	4.42	$3.69 \cdot 10^{-2}$	15.53
Ni₅/Cu	0.69	$3.11 \cdot 10^{-3}$	0.45	$8.31 \cdot 10^{-3}$	1.21

TABLE IV. Conductance and Conductance Oscillations for different metallic multilayers: majority band

Multilayer	Γ	$\Delta\Gamma$	$\Delta\Gamma/\Gamma$ (%)	$\Delta\Gamma_{\max}$	$\Delta\Gamma_{\max}/\Gamma$ (%)
Co₅/Cu	0.29	$1.19 \cdot 10^{-2}$	3.97	$4.21 \cdot 10^{-2}$	14.04
Co₅/Ag	0.28	$1.15 \cdot 10^{-2}$	4.08	$4.01 \cdot 10^{-2}$	14.31
Co₅/Pd	0.18	$1.23 \cdot 10^{-2}$	6.93	$4.13 \cdot 10^{-2}$	23.24
Co₅/Pt	0.19	$8.54 \cdot 10^{-3}$	4.29	$2.51 \cdot 10^{-2}$	12.65
Co₅/Au	0.20	$1.06 \cdot 10^{-2}$	5.08	$3.52 \cdot 10^{-2}$	16.86
Co₁₀/Cu	0.32	$1.08 \cdot 10^{-3}$	3.38	$2.82 \cdot 10^{-2}$	8.80
Co₁₀/Ag	0.32	$1.75 \cdot 10^{-2}$	5.54	$5.73 \cdot 10^{-2}$	18.15
Co₁₀/Pd	0.16	$1.56 \cdot 10^{-2}$	9.78	$3.50 \cdot 10^{-2}$	21.14
Co₁₀/Pt	0.19	$9.02 \cdot 10^{-3}$	4.71	$2.63 \cdot 10^{-2}$	13.73
Co₁₀/Au	0.16	$9.60 \cdot 10^{-3}$	5.95	$2.34 \cdot 10^{-2}$	14.53
Ni₅/Cu	0.51	$7.63 \cdot 10^{-3}$	1.49	$2.39 \cdot 10^{-2}$	4.71

TABLE V. Conductance and Conductance Oscillations for different metallic multilayers: minority band

Multilayer	Γ	$\Delta\Gamma$	$\Delta\Gamma/\Gamma$ (%)	$\Delta\Gamma_{\max}$	$\Delta\Gamma_{\max}/\Gamma$ (%)
Co₅/Cu	0.16	$5.33 \cdot 10^{-3}$	3.31	$1.35 \cdot 10^{-2}$	8.40
Co₅/Ag	0.18	$6.71 \cdot 10^{-3}$	3.62	$2.34 \cdot 10^{-2}$	12.68
Co₅/Pd	0.13	$7.98 \cdot 10^{-3}$	6.04	$1.52 \cdot 10^{-2}$	15.00
Co₅/Pt	0.14	$6.87 \cdot 10^{-3}$	4.81	$2.28 \cdot 10^{-2}$	16.01
Co₅/Au	0.11	$1.25 \cdot 10^{-2}$	10.85	$5.49 \cdot 10^{-2}$	47.45
Co₁₀/Cu	0.18	$6.40 \cdot 10^{-3}$	3.51	$1.62 \cdot 10^{-2}$	8.94
Co₁₀/Ag	0.21	$5.10 \cdot 10^{-3}$	2.46	$1.06 \cdot 10^{-2}$	5.17
Co₁₀/Pd	$9.41 \cdot 10^{-2}$	$1.09 \cdot 10^{-2}$	11.62	$3.15 \cdot 10^{-2}$	33.45
Co₁₀/Pt	0.10	$4.77 \cdot 10^{-3}$	4.69	$1.43 \cdot 10^{-2}$	14.12
Co₁₀/Au	$8.40 \cdot 10^{-2}$	$6.95 \cdot 10^{-3}$	8.27	$1.66 \cdot 10^{-2}$	19.77
Ni₅/Cu	0.47	$4.85 \cdot 10^{-3}$	1.02	$1.38 \cdot 10^{-2}$	2.91

TABLE VI. Conductance and Conductance Oscillations for different metallic multilayers: AF configuration